China Ocean Eng., 2022
DOI: https://doi.org/10.1007/s13344-022-0046-3, ISSN 0890-5487
http://www.chinaoceanengin.cn/ E-mail: coe@nhri.cn

Extreme Value Estimation of Beaufort Sea Ice Dynamics Driven by Global Wind Effects

Chana Sinsabvarodom[a, *], Arvid Næss[b], Bernt J. Leira[a], Wei Chai[c]

[a] Department of Marine Technology, Norwegian University of Science and Technology, Trondheim 7491, Norway

[b] Department of Mathematical Sciences, Norwegian University of Science and Technology, Trondheim 7491, Norway

[c] School of Naval Architecture, Ocean and Energy Power Engineering, Wuhan University of Technology, Wuhan 430070, China

Received December 24, 2021; revised January 14, 2022; accepted February 22, 2022

©2022 The Author(s)

Abstract

The purpose of the present study is to investigate the extreme values of the ice drift speed, which are also considered in the light of the magnitude of the simultaneous wind speed. The relationship between wind speed and ice drift speed is studied. The long-term ice drift data is collected by using local subsurface measurements based on acoustic Doppler current profilers (ADCP) in the Beaufort Sea during the period of 2006−2017. Upward-looking sonars (ULS) are deployed in order to observe the ice thickness as well as to identify events that correspond to open water conditions. The relationship between the ice drift speed and the wind speed is also investigated. It is found that the magnitude of the average ice drift speed is approximately 2.5% of the wind speed during the winter season. Estimation of the extreme values of the ice drift speed is studied by application of the average conditional exceedance rate (ACER) method. It is found that the extreme ice drift speed during the ice melt season (i.e. the summer season) is approximately 20%−30% higher than that during the ice growth season (i.e. the winter season). The extreme ice drift speed can be effectively estimated based on the 2.5% wind speed. Moreover, the extreme ice drift speed can be obtained based on the extreme values of 2.5% of the wind speed based on multiplying with an amplification factor which varies in the range from 1.7 to 2.0 during the growth season, corresponding to increasing return periods of 10, 25, 50 and 100 years.

Key words: ice drift, extreme wind speed, extreme ice-drift speed

Citation: Sinsabvarodom, C., Næss, A., Leira, B. J., Chai, W., 2022. Extreme value estimation of Beaufort Sea ice dynamics driven by global wind effects. China Ocean Eng., doi: https://doi.org/10.1007/s13344-022-0046-3

1 Introduction

Driftting of sea ice takes places as a result of forces caused by the surrounding environmental processes related to wind, current, Coriolis force, tilting of the ocean surface as well as internal contact stresses. The main effects, which dominate the ice drift behavior are those due to wind, current and internal contact stresses, respectively (Campbell, 1965; Steele et al., 1997). Global wind plays an important role in the ice drift, especially for the time scale of days or weeks. Wind blowing across the surface of the sea ice creates drag forces which lead to drifting of the sea ice. The magnitude of the drag force depends on the wind speed as well as on the characteristics of the surface roughness of the ice itself, or the snow cover when present (Leppäranta, 2011). Momentum from the wind is transferred to the sea ice and further down to the water body. Furthermore, both geostrophic ocean currents and tidal currents influence the motion of the oceanic boundary layer (OBL) beneath the ice. The motion of the drifting ice also depends on its inertia, the rheology and the re-distribution of its thickness variation (Leppäranta et al., 2012).

In general, several measurement techniques have been applied in order to observe the ice drift, such as local monitoring (e.g., ADCP), GPS tracking, satellite imaging etc. Each method provides a different precision level corresponding to the sensor characteristics and the payload of the apparatus. GPS tracking can be used to observe the drift motion of sea ice, such as ice floes and icebergs. It provides the drift speed and trajectory data of the relevant objects (Negrel et al., 2018; Yulmetov et al., 2016). At a particular location, local monitoring is an alternative to observation of the sea ice drift in a specific area. Typically, underwater

Foundation item: Open Access funding provided by NTNU Norwegian University of Science and Technology (incl St. Olavs Hospital - Trondheim University Hospital).

*Corresponding author. E-mail: chana.sinsabvarodom@ntnu.no

mooring buoys are employed in order to record the ice thickness, drift speed, temperature, water pressure, etc. Generally, the upward looking acoustic Doppler current profile (ADCP) instrument is installed at the top of mooring buoys in order to observe the ice motion (Teigen et al., 2018; Visbeck and Fischer, 1995). Satellites are commonly used to investigate the climate at larger scales. The information from satellites consists of various types of data such as ice concentration, ice thickness, ice drift speed, etc., in the form of aerial images. The data generally cover quite large areas, while on the other hand this type of data is not characterized by a very high precision level.

In the central Arctic, the ice drift velocity can be observed by using satellite measurements (Spreen et al., 2011). It was found that wind is the major influencing factor in relation to ice drift, which is approximately one to two percent of the mean wind speed above the ice surface during the winters (October−May) from 1992/1993 to 2008/2009. In the range of low wind speeds, a nonlinear relationship is found between the ice drift speed and the wind speed, but the relationship becomes approximately linear within the range of high wind speeds (Thorndike and Colony, 1982). In the Subarctic regions, the wind-induced drift due to the atmospheric circulation causes exchange of sea ice between the Kara Sea and the Central Arctic Ocean (Vinje and Kvambekk, 1991). The ice concentration (i.e. the fraction of areal coverage provided by the ice) is another key parameter that influences the ice drift speed. In general, the three characteristic values represented by ice concentration, ice thickness and ice drift speed are of key importance in any study related to ice drift.

The drift of the sea ice is one of the main parameters associated with the magnitude of the ice loading on ships and offshore structures, and this applies not the least when including dynamic effects (ISO, 2010). The mechanical properties of sea ice inherently depend on the sea ice formation in different areas, which causes uncertainties associated with ice load levels (Sinsabvarodom et al., 2020a). For vertical fixed offshore structures, different ranges of ice drift speeds cause vibration of the strusture, i.e. the so-called ice-induced vibration (IIV). It is an importance issue regarding the safety of structures in ice-covered regions, such as offshore drilling platforms, lighthouses, and bridge piers. The intensive resonant response due to IIV may produce a substantial structural acceleration which can also exceed acceptable levels for people working on the structures (Huang and Liu, 2008; Matlock et al., 1971). Different ice drift speeds can also cause different ice-structure interaction processses, for example, intermittent ice crushing , frequency locking and continuous brittle crushing (ISO, 2010; Määtänen et al., 2012).

For ships and offshore structures operating in drifting ice, increasing drift speed tends to increase the global ice load acting on the surface of the structure. The global ice load on a station-keeping ship in drifting ice can be estimated by using the ice resistance method. Therefore, the drift speed of sea ice becomes a key parameter also for design of mooring lines design in these regions (Sinsabvarodom et al., 2020b). Typically, the mooring system design is based on the limit state approach. Both the short-term and long-term operation conditions must then be considered to achieve a proper design. (API, 1996; DNVGL, 2015). The probability of overloading the mooring systems can be estimated based on the prediction of extreme values corresponding to a specified return period to cover all loading uncertainties.

In the present study, the ice data that are collected by ADCP instruments installed at local mooring stations as part of the Beaufort Gyre exploration project are analyzed. This project was carried out by the Woods Hole Oceanographic Institute (https://www.whoi.edu/). Upwards looking sonars (ULS) are also deployed in order to identify open water events at the different stations. The magnitudes and co-variation of the global wind speed and the ice drift speed are investigated. Subsequently, long-term time series of the ice drift speed and the reduction magnitude of wind speed are applied in order to perform an extreme value analysis based on the average conditional exceedance rate (ACER, 2013) method corresponding to the various exceedance probabilities (which correspond to different return periods).

2 Mooring buoy locations in the Beaufort Sea

Estimation of the ice drift speed is performed by using the time series data from underwater mooring buoys installed in the Beaufort Gyre region. The data is publicly available online at http://www.whoi.edu. Bottom-tethered moorings were installed on the seabed at the four locations illustrated in Fig. 1. Information about the relevant measurement site locations and the recording intervals for each station is listed in Table 1.

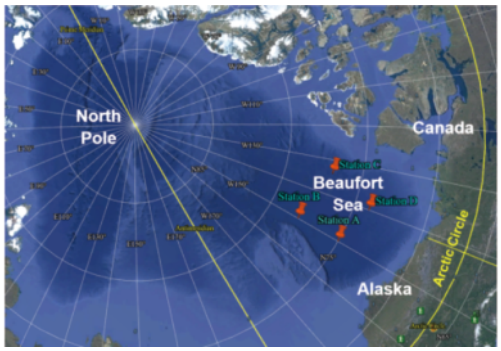

Fig. 1. Sites for collection of data in the Beaufort Gyre region in the Beaufort Sea, the red dots on the map represent the relevant locations (https://earth.google.com/web/).

As illustrated in Fig. 2 and Fig. 3, the mooring buoy at each station is equipped with four instruments: bottom pressure recorder (BPR), a McLane moored profiler (MMP), an upward looking sonar (ULS) and an acoustic Doppler cur-

Table 1 Location and data recording intervals for the different measurement stations

Station	Latitude	Longitude	Water depth (m)	Available data (year)										
				2006−2007	2007−2008	2008−2009	2009−2010	2010−2011	2011−2012	2012−2013	2013−2014	2014−2015	2015−2016	2016−2017
A	750.0270'N	14959.9659'W	3825	−	−	−	−	O	O	−	O	O	O	O
B	7759.8615'N	14957.6695'W	3821	−	−	−	−	O	O	O	O	O	O	−
C	7659.063'N	13957.222'W	3722	−	−	−	−	−	−	−	−	−	−	−
D	740.0007'N	1400.0606'W	3521	O	O	O	O	O	O	O	O	O	O	O

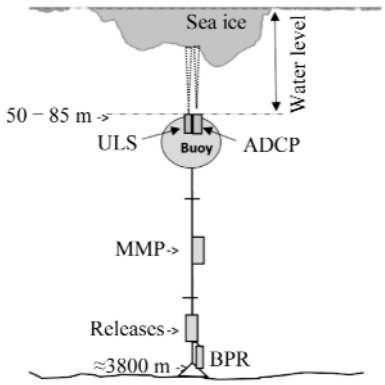

Fig. 2. Illustration of monitoring instruments with corresponding mooring system (Source: https://www2.whoi.edu/site/beaufortgyre/data/mooring-data/mooring-data-description/).

Fig. 3. Subsurface mooring buoy redeployment [Photo by Peter Lourie, October 4, 2016] (Source: https://archives.whoi.edu/beaufortgyre/www.whoi.edu/page.do@pid=155296.html).

rent profiler (ADCP) (Krishfield and Proshutinsky, 2006; Krishfield et al., 2003). Different types of physical properties were recorded by theses instruments. The BPR is employed in order to measure the pressure at the sea bed. The MMP is an autonomous instrument, which is deployed in order to profile the temperature and the salinity of the surrounding water at each station. The Acoustic Doppler Current Profiler (ADCP) is a sonar device, which transmits the acoustic (sound) signals at a fixed frequency with 600 kHz that are reflected by the sea ice. The returned echo signal is then transformed into ice velocity. The upward-looking sonar (ULS) is used in order to observe the draft of the sea ice cover (Sinsabvarodom et al., 2019).

3 Theoretical background

In this section, characterization of ice drift behavior and corresponding analysis methods are presented. The magnitude and direction of the ice drift are calculated from its velocity components, which were monitored by means of the ADCP equipment. The velocity vectors in the horizontal plane are employed in order to predict the extreme values of the ice drift velocity by utilization of the average conditional exceedance rate (ACER) method.

3.1 Calculation of horizontal ice drift speed and direction

The speed and direction of the ice drift are ideally corresponding to a Brownian motion. The external forces that influence the ice drift are generated by the surrounding environment. The ADCP instrument employs a series of acoustic transducers that emit and receive pings through the above sea ice cover at many different angles simultaneously. This allows to determine the speed and direction of the object. The primary records from the ADCP measurements are adjusted for speed of sound and depth variations relative to the vertical center. It is converted to Earth-referenced velocities and corrected for magnetic declination (https://www2.whoi.edu/site/beaufortgyre/data/mooring-data/mooring-data-description/). In the present research, the vector components of the ice drift velocity during each hour, t, referred to a three-dimensional earth coordinate system in terms of north−south, east−west, and up−down with origin just above the respective observation point. The magnitude of the ice drift speed in the horizontal direction, $v_h(t)$ is expressed by Eq. (1):

$$v_h(t) = \sqrt{v_N(t)^2 + v_E(t)^2}, \tag{1}$$

where $v_N(t)$ and $v_E(t)$ are the horizontal velocity vectors in the directions of the latitude (N) and the longitude (E), respectively. The direction of the ice drift is specified in terms of rotation angle, θ, corresponding to a polar coordinate system with origin at the observation station. The rotational angle, θ can obtain values in the range from 0° to 360°. It is calculated based on the components of the velocity vector, i.e. $v_N(t)$ and $v_E(t)$, as given in Eq. (2):

$$\theta = \arctan\left(\frac{v_N}{v_E}\right). \tag{2}$$

3.2 Extreme value prediction

The objective of the extreme value analysis is to provide a prediction of the largest ice drift speed corresponding to specified probability of exceedance levels (or equivalently return periods). The ice drift data observed at each station is then considered to represent an underlying stochastic process. The relevant time interval, for which the ice drift speed, V, is considered, and taken to be $[0, T]$.

In the present study, prediction of the extreme value of the ice drift speed is performed by means of the average

conditional exceedance rate (ACER) method, which is a numerical approach in order to estimate the extreme values by constructing the corresponding ACER functions (Næss and Gaidai, 2009) of different order, k. It can be applied to analyze time series realizations of a stochastic process for both stationary and non-stationary data sets. The principle and development of extreme value estimation by means of ACER functions are described in more detail by Næss and Gaidai (2009) and Næss et al. (2013). These functions are applied as a basis for developing the function given in Eq. (3):

$$P(\eta) \approx \exp[-(N-k+1)\hat{\varepsilon}_k(\eta)], \tag{3}$$

where $\hat{\varepsilon}_k(\eta)$ is the empirical ACER function of order, k as given in Eq. (4). Although increasing accuracy is obtained for increasing order k of the ACER function, the number of data points for calculation of $\hat{\varepsilon}_k(\eta)$ is reduced according to the corresponding numerical scheme. Generally, the ACER functions of level η are highly regular in the tail region, assumed to apply for levels beyond a suitably chosen tail marker η_0.

$$\varepsilon_k(\eta) \approx q_k \exp[-a_k(\eta-b_k)^{c_k}],\ \eta \geqslant \eta_0, \tag{4}$$

where a_k, b_k, c_k and q_k are parameter constants, that are dependent upon the order, k. The valid range for the values of the ACER coefficients are $a_k > 0$, $b_k \leqslant \eta_0$ and $c_k > 0$.

When the values of a_k, b_k, c_k and q_k are obtained, the extrapolation scheme described by Eq. (4) can be applied to provide reasonably accurate estimation of deep tail extreme values needed for obtaining long return period design values. The optimal values of the parameters are obtained by minimizing the mean square error as expressed in Eq. (5).

$$F(a_k,b_k,c_k,q_k) = \sum_{i=1}^{M} \rho_j \left| \ln[\hat{\varepsilon}_k(\eta_i)] - \ln q + a(\eta_i - b)^c \right|^2, \tag{5}$$

where ρ_i is a weight factor to enhance the influence from the most reliable data points. η_i, $i = 1, \cdots, M$ are levels of the ACER function, for which data points are available. The data fitting here is based on $\rho_i = (\ln CI^+(n_i) - \ln CI^+(n_i))^{-2}$ where CI^+ and CI^- are the bounds of the 95% confidence interval (CI). By fixing the values of b_k and c_k parameters, obtaining optimal values of a_k and $\ln q_k$ parameters reduces to a standard weighted linear regression problem in terms of $\rho_i, y_i = \ln[\hat{\varepsilon}_k(\eta_i)]$ and $x_j = (\eta_j - b)^c$. Specifically, the optimal values of a_k and $\ln q_k$ are expressed by Eqs. (6) and (7).

$$a_k^*(b_k,c_k) = -\frac{\sum_{i=1}^{M} \rho_i (x_i - \bar{x})(y_i - \bar{y})}{\sum_{i=1}^{M} \rho_i (x_i - \bar{x})^2}, \tag{6}$$

$$\ln\left[q_k^*(b_k,c_k)\right] = \bar{y} + a_k^*(b_k,c_k)\,\bar{x}, \tag{7}$$

where $\bar{x} = \sum_{i=1}^{M} \rho_i x_i \Big/ \sum_{i=1}^{M} \rho_i$ and $\bar{y} = \sum_{i=1}^{M} \rho_i y_i \Big/ \sum_{i=1}^{M} \rho_i$.

The optimal values of b_k and c_k parameters are now found by means of the Levenberg-Marquardt method. The final ACER function can be estimated from the fitted curve in order to optimize the confidence interval of the predicted value. The selection of threshold values for prediction of the extreme value is not a very critical issue, however, they should still be chosen with some care. Finally, with the assistance of the efficient extrapolation scheme, which is based on the assumption of regularity of the ACER functions with respect to the deep tail regions, the extreme distribution of ice drift speed can be obtained.

In the present study, the analysis procedure starts by obtaining time series of the ice drift velocity and the ice thickness from the ADCP and the ULS measurements. After that, classification of the ice cover is applied in order to distinguish between the presence of ice versus open water. Calculation of both ice drift speed and direction are required in order to interpret the collected time-series. The seasonal dependence of ice drift behavior for the growth season versus the melting season is investigated. The influence and relationship between the wind speed and the ice drift speed are studied. Subsequently, anextreme value analysis is performed based on the different steps that are illustrated in Fig. 4.

4 Results

4.1 Joint variation of wind speed and ice drift speed

Long-term ice drift data are collected from the ADCP measurements which are recorded once in an hour. Data records at Stations A, B and D are available. Unfortunately, for Station C, no data is obtained. The ice data record starts on 1st October of each year corresponding to the specified start of the winter season according to the Canadian regulations. The ADCP measurements provide the velocity components in three orthogonal directions as referred to the global Cartesian coordinate system. The calculation of horizontal ice drift speed is carried out by means of Eq. (1). Long-term data of ice drift time series are considered as a basis for the extreme value analysis. Due to different time intervals for the records from the ULS and the ADCP measurements, data points of ice thickness at the same time instants as those available for the ice drift speed are selected. This also allows identification of open water conditions, which correspond to the ice thickness from the ULS measurement being equal to zero.

The wind is generally assumed to play an important role in relation to the magnitude and direction of the ice drift in the oceans (Leppäranta, 2011). The exposed area of the ice surface is subjected to aerodynamic drag forces caused by the wind-induced airflow. The present study considers the joint variation of the ice drift speed and the seasonal wind speed. The wind speed data were obtained from the Ventusky web application, which has been developed by the company InMeteo. This web application is a platform for

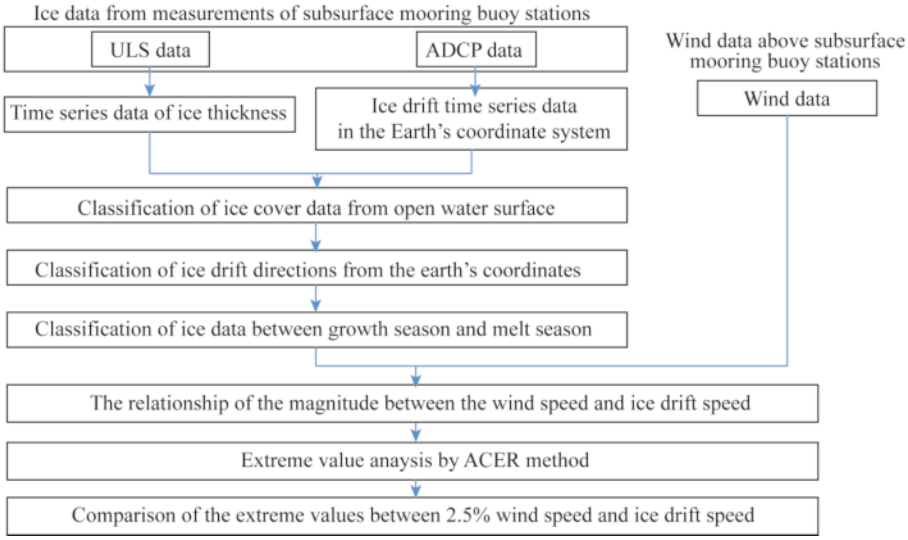

Fig. 4. Flowchart of the steps related to the extreme value analysis.

weather prediction and visualization of metorological data at a global scale (https://www.ventusky.com/). A numerical model for weather prediction has been developed by the Canadian Meteorological Centre, CMC. Usually, the calculations are performed every 3 hours with a grid resolution of roughly 25 km. The data is updated every 12 hours and the web application has been available since 2016. The wind speed at 10 m above the water surface at the ADCP measurement stations is employed in order to study the joint variation of the wind and ice drift speeds. The data points for the ice drift speed that coincide in time with the more sparse data points for the wind speed are selected as a basis for the analysis. Data records obtained from ADCP measurement in the year 2016−2017 were available only for Stations A and D, and the distance between these two stations is 316.8 km.

From the recorded time series, it is found that there are seasonal differences in relation to the joint variation of the wind speed and the ice drift speed during the growth season versus the melt season. The thickness of the sea ice will have a physical effect on the dynamics of the ice drift process owing to the inertia forces and rheological properties (Leppäranta et al., 2012). Typically, the ice drift speed is approximately 2%−3% of the surface wind speed in the Arctic Ocean (Kawaguchi et al., 2019; Leppäranta et al., 2012). In the Beaufort Gyre, it is presently found that the magnitude of the ice drift speed for both Stations A and D during the winter season is about 2.5% of the wind speed. Examples of scatter plots between the ice drift speed and 2.5% of the wind speed during the growth season and the melt season are shown in Fig. 5. The ice drift speed exhibits a higher correlation with 2.5% of the wind speed during the growth season from October to June than for the summer season from June to August. The development of the ice thickness during the growth season and the melt season can be clearly observed from the ULS measurements. The sea ice starts to form in October and reaches the highest thickness around June. Subsequently, the ice thickness starts to decrease and mainly disappears around the end of August. The time series of the ice drift speed, ice thickness and 2.5% of the wind speed from the field measurements are shown in Fig. 6.

Furthurmore, formation of the ice can also be obsered form satellite images. However, such observations have some limitation during cloudy weather, when the sky is blocked. Some satellite images obtained during 2016–2017 are shown in Fig. 7. The most serious ice conditions are seen to take place in June, while the ice tends to disappear in August.

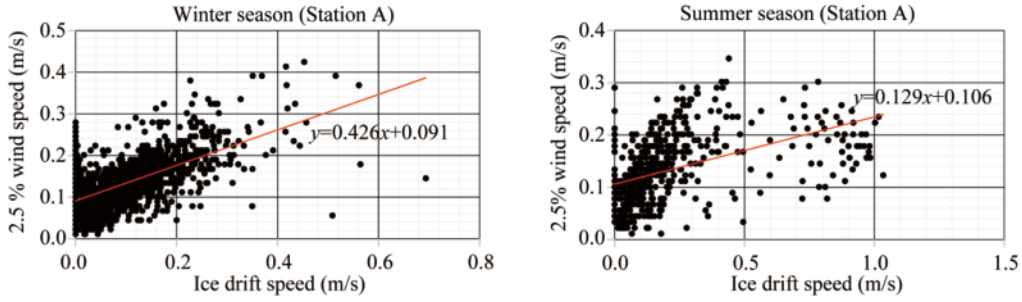

Fig. 5. Relationship between ice drift speed and 2.5% of the wind speed at Station A during the growth season and the melt seasion during 2016−2017.

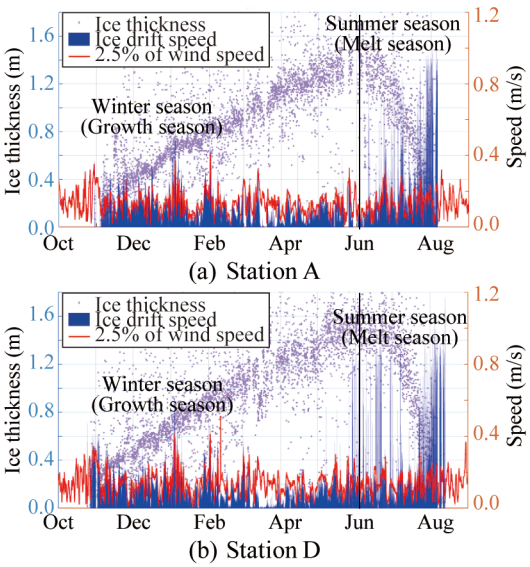

Fig. 6. Time series of ice drift speed and 2.5% of the wind speed together with the ice thickness variation during 2016−2017 for Station A (a) and Station D (b).

4.2 Extreme value analysis

Extreme value analysis of ice drift speed at each station is performed in order to estimate the characteristic largest drift speed corresponding to given return periods. Generally, high drift speed is associated with an ice failure mechanism (when interacting with a structure) referred to as continuous brittle crushing. This applies in particular for the case of dynamic ice action on vertical fixed offshore structures (ISO, 2010). For station-keeping of ships in ice, higher drift speeds imply higher global ice loading which is reflected by the so-called ice resistance approach (Sinsabvarodom et al., 2021). The extreme value of the ice drift speed (corresponding to a given design return period) implies the largest value of the ice loading on ships and/or offshore structures during the same period.

Extreme value analysis by means of the ACER method is based on the empirical ACER functions, $\hat{\varepsilon}_k(\eta)$, which are plotted versus the amplitude of ice drift speed for different orders, k. Examples of ACER functions for the ice drift speed for Station D corresponding to various values of k in the growth and melt seasons are illustrated in Fig. 8a. For the wind, the ACER functions of the time series of 2.5% of the wind speed from 2016−2017 are determined for various k as illustrated in Fig. 8b. The yearly wind data are employed for the analysis because the wind speed data does not clearly differentiate with respect to seasonal variations of the sea ice. This can also be seen from the magnitude of the wind speed in the time series illustrated in Fig. 6. However, It still seems that the wind speeds are higher in November to March than from April to October.

From the ACER function plots $b_k \leqslant \eta_0$, the effect of dependence between data points can be quantified. The effect of this dependence gradually diminishes when the levels of the ice drift speed and the wind speed increase. In the uppermost tail, the effect of this dependence vanishes completely. Coalescence of the functions in the tail region allows application of the lower order ACER functions for extrapolation proposes. While the higher orders of the ACER functions provide a closer fit to the extreme value distribution inherent in the data, the number of data points which are available for estimation purposes are reduced according to the numerical estimation scheme. Hence, the lower order ACER functions may give more robust extrapolation results.

For the present analysis, the values of k are selected for the purpose of extreme value prediction corresponding to the number of collected data points in the long-term series. The bounds of the confidence interval estimated from the data, i.e. CI^-,CI^+ correspond to the 95% confidence interval. The 100-year return period levels are estimated in the present analysis. The extreme values corresponding to these horizontal lines are estimated by specifying a target exceedance probability (or equivalently: a return period) which is set equal to the probability level of the ACER function as given by Eq. (4). The ACER functions can be extrapolated to determine the corresponding extreme value of the ice drift speed (for the 100-year return period) as illustrated by the red horizontal lines in Fig. 9.

The results of the extreme values for the ice drift speed and 2.5% of the wind speed for each station corresponding to a range of different return periods ranging from 10 to 100 yeas are listed in Table 2.

5 Discussion

5.1 Relationship between the global wind speed and ice drift speed

In the Beaufort Sea, the sea ice tends to drift at approx-

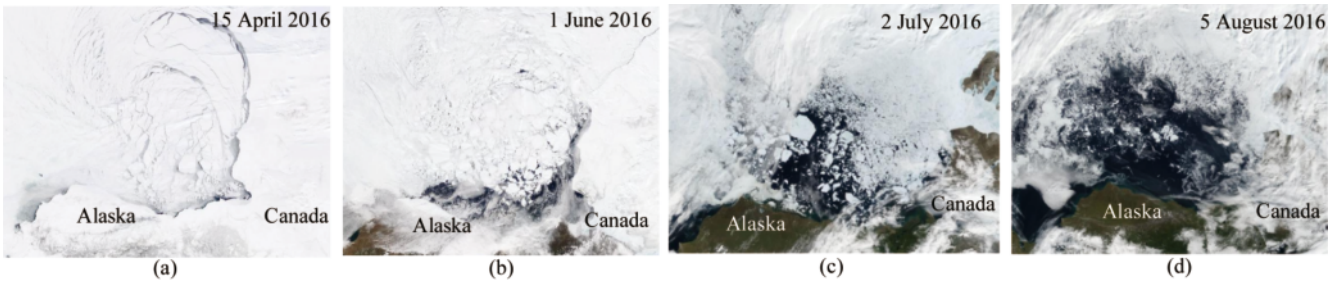

Fig. 7. Satellite images from observation area in the Beaufort Sea (source: https://zoom.earth).

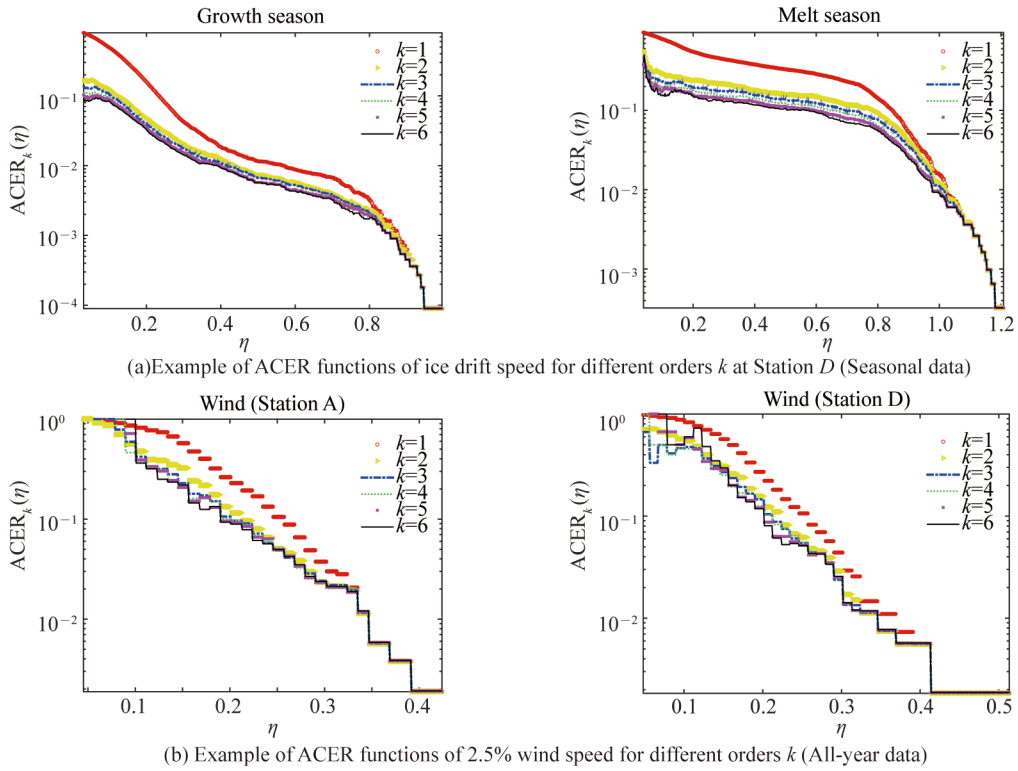

(a)Example of ACER functions of ice drift speed for different orders k at Station D (Seasonal data)

(b) Example of ACER functions of 2.5% wind speed for different orders k (All-year data)

Fig. 8. Examples of ACER functions of ice drift speed and 2.5% of the wind speed.

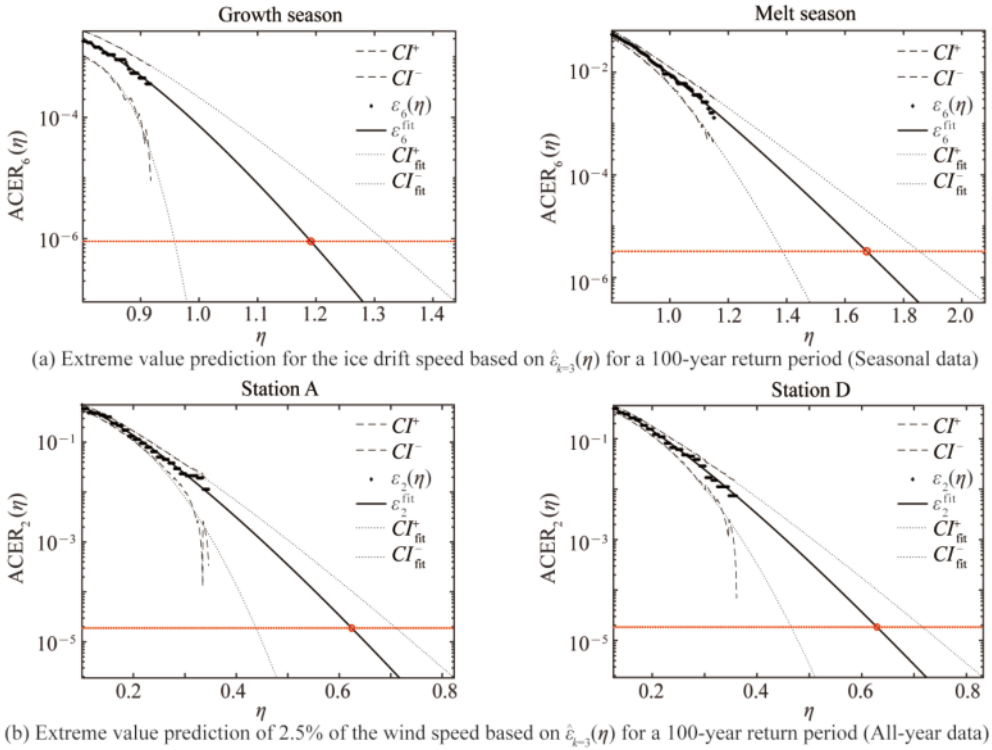

(a) Extreme value prediction for the ice drift speed based on $\hat{\varepsilon}_{k=3}(\eta)$ for a 100-year return period (Seasonal data)

(b) Extreme value prediction of 2.5% of the wind speed based on $\hat{\varepsilon}_{k=3}(\eta)$ for a 100-year return period (All-year data)

Fig. 9. Extreme value prediction by the ACER method.

imately 2.5% of the global wind speed (as referred to a height of 10 m above the sea surface). The 2.5%-value is similar to the rule of thumb which was suggested by Leppäranta (2011). Moreover, it is found that the sea ice trends to provide strong correlation with the fraction of wind speed in the growth season as illustrated in Fig. 5a. Then the degree of correlation physically tends to diminish when sea ice starts to melt. The sea ice tends to drift faster

Table 2 Results of the extreme value prediction by ACER method

Return period (year)	Extreme ice drift speed (m/s)						Extreme wind speed (m/s)	
	Station A		Station B		Station D		Station A	Station D
	Growth season	Melt season	Growth season	Melt season	Growth season	Melt season	2.5% wind speed	2.5% wind speed
10	1.08	1.34	0.99	1.39	1.03	1.39	0.52	0.52
25	1.14	1.38	1.03	1.44	1.06	1.44	0.57	0.56
50	1.17	1.42	1.06	1.48	1.07	1.48	0.60	0.59
100	1.21	1.45	1.09	1.52	1.09	1.52	0.62	0.61

in the summer or melt season. The slope of linear fitting between the ice drift speed and 2.5% wind speed is flatter due to the faster drift speed. This can be observed in Fig. 5b. The drift speed is higher in the summer season owing to melting of the sea ice. This leads to ice free intervals on the water surface as shown on the satellite images in Fig. 7. The internal stress between the ice floes is then reduced.

5.2 Extreme value of ice drift speed

The extreme values of the ice drift speed during the winter season and the melt season are estimated by means of the ACER method. A comparison between the extreme values of the ice drift speed corresponding respectively to 10-, 25-, 50- and 100-year return periods at each station is shown in Fig. 10. The extreme value of the ice drift speed during the winter season for Station A is higher than that for Stations D and B, respectively. The extreme values for the different stations (corresponding to the same return periods) vary by approximately 12%. Concerning the extreme values for the ice drift speed during the melt season, Station D exhibits higher extreme values than Stations B and A, respectively. The differences in extreme values between the three stations are approximately 5%.

The extreme values are next normalized with the observed maximum values during the recording period in order to study the relative increase corresponding to increasing return periods. The percentwise increase of the ice drift speed (relative to the maximum observed value) is seen to be approximately 10%, 15%, 20%, and 25% for return periods of 10-, 25-, 50- and 100-year, respectively, as illustrated by Fig. 11.

The wind during the winter season has a strong influence on the ice drift. The magnitude of the ice drift speed is approximately 2.5% of the wind speed in the Beaufort Sea during this season. In this section, the relationship between the extreme values of the ice drift speed and 2.5% of the

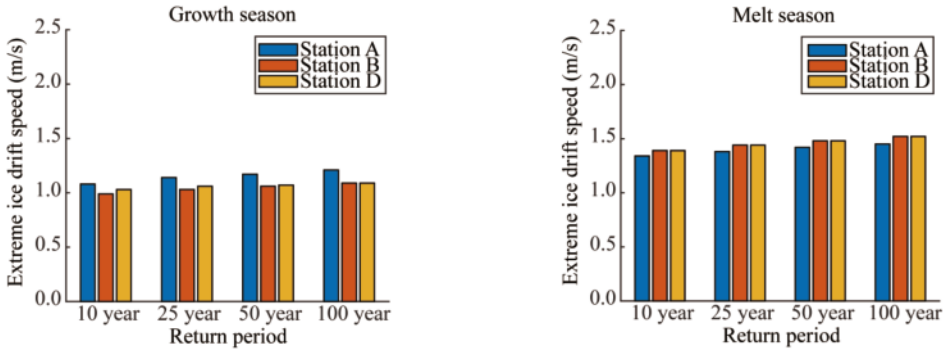

Fig. 10. Comparison of extreme ice drift speeds corresponding to different return periods calculated by the ACER method for the growth season versus the melt season.

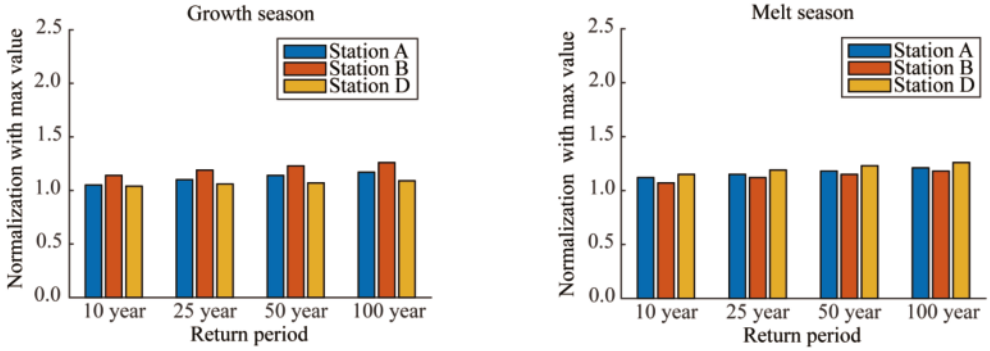

Fig. 11. Normalization of extreme value ice drift speeds with maximum observed values during the recording period for the growth and melt seasons at each station.

wind speed is investigated. It is found that a rough estimate of the extreme ice drift speed can be obtained based on 2.5% of the wind speed. The extreme values of the ice drift speed are typically higher than 2.5% of the wind speed by approximately a factor of 1.7−2.0 as illustrated by Fig. 12. This is of significant advantage since the wind data are generally available via the common weather forecast. Accordingly, the 2.5% value of the extreme wind speed can be employed to predict the extreme ice drift speed by multiplication with an amplification factor of around 1.7−2.0.

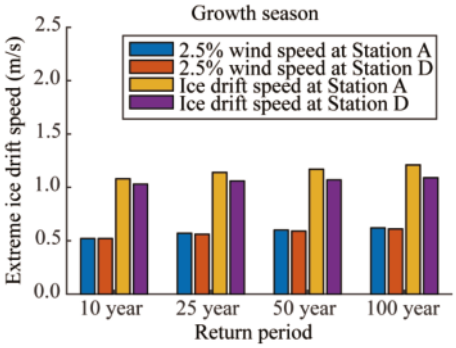

Fig. 12. Comparison of the extreme ice drift speed with the 2.5% wind speed for each station corresponding to four different return periods.

6 Conclusions

The upward looking sonar (ULS) is beneficial in order to classify data associated with ice cover thickness and for joint recording of data together with the acoustic Doppler current profiler (ADCP). These combined records allow quite accurate estimation of the existing sea ice on the water surface. The ACER method is applied to estimate the extreme values of the ice drift speed in the Beaufort Sea. According to the present study, the following conclusions can be drawn.

(1) The ice drift speed is approximately 2.5% of the global wind speed (as referred to a height of 10 m above the water surface) during the winter season in the Beaufort Sea.

(2) The ice drift speed has a stronger correlation with the 2.5% wind speed during the growth season versus the melt season.

(3) The extreme values of the ice drift speed in the melt season corresponding to different return periods have higher values than those for the growth season, and the speeds are typically being increased by around 20%−30%.

(4) The observed extreme values of the ice drift speed are higher than the 2.5% wind speed during the winter season by a factor of approximately 1.7−2.0.

Acknowledgments

This work was supported by the NTNU Oceans Pilot project **"**Risk, reliability and ice data in the Arctic marine environment". We sincerely acknowledge the various sources of the data used in this research. The data from ice measurements were collected and published by the Beaufort Gyre Exploration Program based at the Woods Hole Oceanographic Institution (http://www.whoi.edu/beaufortgyre) in collaboration with researchers from Fisheries and Oceans Canada at the Institute of Ocean Sciences. The wind data was available from Ventusky web application, which has been developed by InMeteo company (https://www.ventusky.com) and Satellites immage above obsevation area in the Beaufort Sea from Zoom Earth Website (https://zoom.earth).

Right and permissions

Open Access This article is licensed under a Creative Commons Attribution 4.0 International License, which permits use, sharing, adaptation, distribution and reproduction in any medium or format, as long as you give appropriate credit to the original author(s) and the source, provide a link to the Creative Commons licence, and indicate if changes were made. The images or other third party material in this article are included in the article's Creative Commons licence, unless indicated otherwise in a credit line to the material. If material is not included in the article's Creative Commons licence and your intended use is not permitted by statutory regulation or exceeds the permitted use, you will need to obtain permission directly from the copyright holder. To view a copy of this licence, visit http://creativecommons.org/licenses/by/4.0/.

References

ACER, 2013. *The ACER User Resources*. https://folk.ntnu.no/arvidn/ACER/.

API, 1996. *Recommended Practice for Design and Analysis of Station-keeping Systems for Floating Structures*, American Petroleum Institute.

Campbell, W.J., 1965. The wind-driven circulation of ice and water in a polar ocean, *Journal of Geophysical Research*, 70(14), 3279–3301.

DNVGL, 2015. *Position Mooring*, DNVGL-OS-E301, DNV GL, Oslo.

Huang, G. and Liu, P., 2008. A dynamic model for ice-induced vibration of structures, *Journal of Offshore Mechanics and Arctic Engineering*, 131(1), 011501.

ISO, 2010. ISO 19906:2010-Petroleum and natural gas industries–Arctic offshore structures.

Kawaguchi, Y., Itoh, M., Fukamachi, Y., Moriya, E., Onodera, J., Kikuchi, T. and Harada, N., 2019. Year-round observations of sea-ice drift and near-inertial internal waves in the Northwind Abyssal Plain, Arctic Ocean, *Polar Science*, 21, 212–223.

Krishfield, R. and Proshutinsky, A., 2006. *BGOS ULS Data Processing Procedure*, Woods Hole Oceanographic Institution.

Krishfield, R., Toole, J. and Proshutinsky, A., 2003. BGFE 2003–2004 MMP EMCTD and ACM Data Processing Procedures.

Leppäranta, M., 2011. *The Drift of Sea Ice*, second ed., Springer, Berlin, Heidelberg.

Leppäranta, M., Oikkonen, A., Shirasawa, K. and Fukamachi, Y., 2012. A treatise on frequency spectrum of drift ice velocity, *Cold Regions Science and Technology*, 76–77, 83–91.

Määtänen, M., Løset, S., Metrikine, A., Evers, K.U., Hendrikse, H.,

Lonoy, C., Metrikin, I., Nord, T. and Sukhorukov, S., 2012. Novel ice induced vibration testing in a large-scale facility: Deciphering ice induced vibrations, Part 1, *Proceedings of the 21st IAHR International Symposium on Ice*: *Ice Research for a Sustainable Enviroment*, Dalian University of Technology Press, Dalian, China.

Matlock, H., Dawkins, W.P. and Panak, J.J., 1971. Analytical model for ice-structure interaction, *Journal of the Engineering Mechanics Division*, 97(4), 1083–1092.

Næss, A. and Gaidai, O., 2009. Estimation of extreme values from sampled time series, *Structural Safety*, 31(4), 325–334.

Næss, A., Gaidai, O. and Karpa, O., 2013. Estimation of extreme values by the average conditional exceedance rate method, *Journal of Probability and Statistics*, 2013, 797014.

Negrel, J., Gerland, S., Doulgeris, A.P., Lauknes, T.R. and Rouyet, L., 2018. On the potential of hand-held GPS tracking of fjord ice features for remote-sensing validation, *Annals of Glaciology*, 59, 173–180.

Sinsabvarodom, C., Chai, W., Leira, B.J., Høyland, K.V. and Næss, A., 2019. Probabilistic assessment of ice rose diagrams for ice drift in the Beaufort Sea, *Proceedings of the 25th International Conference on Port and Ocean Engineering under Arctic Conditions*.

Sinsabvarodom, C., Chai, W., Leira, B.J., Høyland, K.V. and Næss, A., 2020a. Uncertainty assessments of structural loading due to first year ice based on the ISO standard by using Monte-Carlo simulation, *Ocean Engineering*, 198, 106935.

Sinsabvarodom, C., Leira, B.J., Chai, W. and Næss, A., 2020b. Extreme value estimation of mooring loads based on station-keeping trials in ice, *Proceedings of ASME 2020 39th International Conference on Ocean*, *Offshore and Arctic Engineering*, ASME, Fort Lauderdale, Florida.

Sinsabvarodom, C., Leira, B.J., Chai, W. and Næss, A., 2021. Short-term extreme mooring loads prediction and fatigue damage evaluation for station-keeping trials in ice, *Ocean Engineering*, 242, 109930.

Spreen, G., Kwok, R. and Menemenlis, D., 2011. Trends in Arctic sea ice drift and role of wind forcing: 1992–2009, *Geophysical Research Letters*, 38(19), L19501.

Steele, M., Zhang, J.L., Rothrock, D. and Stern, H., 1997. The force balance of sea ice in a numerical model of the Arctic Ocean, *Journal of Geophysical Research*: *Oceans*, 102(C9), 21061–21079.

Teigen, S.H., Lindvall, J.K., Samardzija, I. and Hansen, R.I., 2018. Station-keeping trials in ice: Ice and metocean conditions, *Proceedings of ASME 2018 37th International Conference on Ocean*, *Offshore and Arctic Engineering*, American Society of Mechanical Engineers, Madrid, Spain.

Thorndike, A.S. and Colony, R., 1982. Sea ice motion in response to geostrophic winds, *Journal of Geophysical Research*: *Oceans*, 87(C8), 5845–5852.

Vinje, T. and Kvambekk, Å.S., 1991. Barents Sea drift ice characteristics, *Polar Research*, 10(1), 59–68.

Visbeck, M. and Fischer, J., 1995. Sea surface conditions remotely sensed by upward-looking ADCPs, *Journal of Atmospheric and Oceanic Technology*, 12(1), 141–149.

Yulmetov, R., Marchenko, A. and Løset, S., 2016. Iceberg and sea ice drift tracking and analysis off north-east Greenland, *Ocean Engineering*, 123, 223–237.